Visualization and Quantification of 3-Dimensional Stereotactic Surface Projections for ^{18}F-Flutemetamol PET Using Variable Depth

Johan Lilja[1,2], Lennart Thurfjell[1,3], and Jens Sörensen[2]

[1]GE Healthcare, Uppsala, Sweden; [2]Nuclear Medicine and PET, Department of Surgical Sciences, Uppsala University, Uppsala, Sweden; and [3]Institute of Neuroscience and Physiology, The Sahlgrenska Academy at the University of Gothenburg, Gothenburg, Sweden

Three-dimensional stereotactic surface projection (3D-SSP) is a widely used method for the analysis of clinical ^{18}F-FDG brain studies. However, for PET amyloid scans the use of 3D-SSP is challenging because of nonspecific uptake in white matter. Our objective was to implement a method for 3D-SSP quantification and visualization of ^{18}F-flutemetamol images that avoids extraction of white matter signal. **Methods:** Triangulated brain surface models were extracted from a T1-weighted MR template image. Using an ^{18}F-flutemetamol–negative template, a maximum depth for each vertex on the surface models was calculated to avoid extraction of white matter. The method was evaluated using ^{18}F-flutemetamol images from 2 cohorts. Cohort 1 consisted of 105 healthy volunteers and was used to create a normal database for each reference region. Cohort 2 consisted of 171 subjects including patients with Alzheimer disease and mild cognitive impairment and healthy volunteers. Images were spatially normalized using an adaptive template registration method, and SUV ratio 3D-SSP values were computed using the pons and cerebellar cortex as reference regions. Images from cohort 2 were then compared with the normal database and classified into negatives and positives, based on a calculated *z* score threshold. The results were compared with consensus visual interpretation results from 5 trained interpreters blinded to clinical data. **Results:** With the pons as the reference region, the optimal *z* score threshold was 1.97, resulting in an overall agreement with visual interpretation results in 170 of 171 images (99.42%). With the cerebellar cortex as the reference region, the optimal *z* score threshold was 2.41, with an overall agreement with visual interpretation in 168 of 171 images (98.25%). **Conclusion:** Variable-depth 3D-SSP allows computation and visualization of ^{18}F-flutemetamol 3D-SSP maps, with minimized contribution from white matter signal while retaining sensitivity in detecting gray matter signal.

Key Words: Alzheimer's disease; positron emission tomography; brain mapping; stereotactic surface projections; flutemetamol; amyloid

J Nucl Med 2016; 57:1078–1083
DOI: 10.2967/jnumed.115.169169

Alzheimer disease (AD) has a high prevalence among the elderly population, and the incidence is rising (*1*). Amyloid accumulation in the brain is a hallmark of AD and therefore also a relevant target of pharmacologic therapy (*2*). PET contributes to antemortem diagnosis of AD with 2 different classes of approved radiopharmaceuticals, ^{18}F-FDG for visualization of regional brain metabolism and amyloid-binding tracers. Pittsburgh compound B (^{11}C-PIB) (*3*) belongs to the second class and binds to amyloid plaques in the brain and has been used for the in vivo assessment of amyloid deposits in the brain in AD research. Because of the logistic limitations due to the short half-life of ^{11}C, amyloid tracers using the longer-lived radiolabel ^{18}F have been developed: ^{18}F-florbetapir (*4,5*), ^{18}F-florbetaben (*6,7*), and ^{18}F-flutemetamol (*8,9*), all approved in the United States and European Union, and the late-stage investigational amyloid imaging agent NAV4694 (*10*).

Evaluation of AD pathology using amyloid tracers and PET in clinical routine currently relies mainly on visual interpretation, and all approved agents are currently recommended to be assessed by visual image interpretation techniques as part of the approved instructions for use. Quantitative methods are relatively elaborate and are mainly used in research. In general, quantification requires a work sequence of coregistration of PET image to MR image, intensity normalization of PET activity to a reference region in either the pons or the cerebellum, outlining of relevant anatomic regions, and comparison of acquired regional values to a normal database. Reporting of image findings is therefore primarily text-based, with occasional images of raw PET data.

Three-dimensional stereotactic surface projections (3D-SSP) of ^{18}F-FDG brain studies have become widespread for analysis and reporting. 3D-SSP of ^{18}F-FDG is able to reveal image patterns associated with AD (*11*). A previous study comparing quantification using 3D-SSP with visual assessment for detection of mild cognitive impairment and AD showed that 3D-SSP gave more accurate results, especially for the novice interpreter (*12*).

The 3D-SSP method defines a large number of points on a brain surface model defined in a standard stereotactic space for which each point is associated with a vector perpendicular to the brain surface (surface normal) (Fig. 1). After registration of a patient's PET image to the stereotactic space (spatial normalization), the method determines the maximum cortical uptake for each surface point by sampling the registered image in the inverse direction of the surface normal into the brain to a predefined depth. The maximum value sampled along each ray is then mapped to the corresponding surface point.

Both ^{18}F-FDG and amyloid PET images show changes in cortical uptake associated with AD. However, although ^{18}F-FDG shows highest uptake in normal cortical gray matter, all current amyloid tracers show significant uptake in gray matter only when

Received Nov. 3, 2015; revision accepted Jan. 29, 2016.
For correspondence or reprints contact: Johan Lilja, Akademiska sjukhuset, 751 85 Uppsala, Sweden.
E-mail: johan.lilja@radiol.uu.se
Published online Feb. 16, 2016.

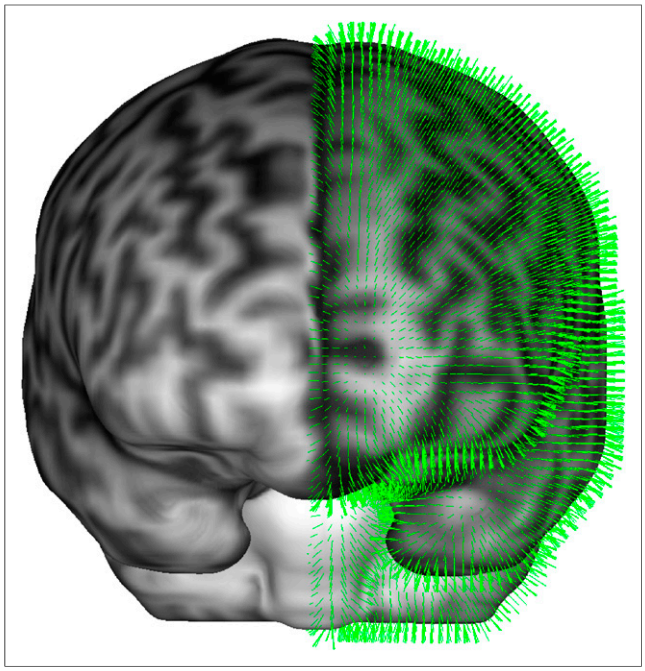

FIGURE 1. Illustration of subset of all normal vectors defined on brain surface model.

amyloid is present. However, images based on amyloid tracers also show nonspecific binding in white matter, and in amyloid-negative (Aβ−) images activity in white matter is higher than in cortical gray matter.

The original 3D-SSP method samples data to a predefined depth that is the same across the brain cortex (*11*). Although this approach works well for ^{18}F-FDG, it may be problematic when applying 3D-SSP to images obtained using PET amyloid tracers because of the potential that white matter uptake is included if measuring too deep into the cortex while measuring too shallow may cause loss in sensitivity. Hence, for amyloid tracers it is important to have a method that can successfully project cortical uptake but at the same time minimize the risk for blending in signal emanating from white matter. With access to an MR image, the subject's brain cortical thickness can be calculated directly and used for the appropriate depth definition. However, for robust and routine automated analysis of amyloid PET in the clinic a method independent of MR might be preferable.

Our objective was to develop a method for 3D-SSP quantification and visualization of ^{18}F-flutemetamol images that avoids white matter signal contamination and without dependence on MR information.

MATERIALS AND METHODS

Pooled data from 6 previous clinical studies of ^{18}F-flutemetamol were used. Approvals for the studies were obtained from the Ethical Committees of the participating centers, and written informed consent was obtained from all participants. Data were grouped into 2 cohorts: a healthy cohort (cohort 1) comprising 105 healthy volunteers from 3 studies (*9,13,14*); and a test cohort (cohort 2) comprising 33 patients with clinically probable AD, 80 patients with mild cognitive impairment, and 59 healthy volunteers, giving a total of 172 subjects.

Data in cohort 2 were from a phase-III study in which the effectiveness of an electronic training program for interpretation of ^{18}F-flutemetamol images was assessed (*15*).

^{18}F-flutemetamol PET images were acquired as 6 × 5 min frames starting 85–90 min after injection of approximately 185 MBq of ^{18}F-flutemetamol. For this study, the first 4 frames were summed to yield an image corresponding to a 20-min static scan.

Blinded Image Evaluation (BIE)

In a previously performed BIE study (*15*), each subject's PET image was interpreted separately by 5 interpreters who were each blinded to all subjects' clinical information. Interpreters were trained using a computer-based electronic training program. Images were reviewed in color, typically using a Sokolov or Rainbow color scale. The interpreters were trained to review the following regions: frontal, posterior cingulate/precuneus, lateral temporal, inferior parietal, and striatum. Images were scaled to place the uptake in the pons at 90% of intensity maximum. Images were then defined as amyloid-positive (Aβ+) if any region had an abnormal appearance, that is, the intensity in any gray matter region listed above was clearly in excess of 50% of the image's maximum intensity or there was an absence of a well-defined sulcal/gyral pattern. The results of the BIE were available for all scans in cohort 2. In this study, most visual read results were used to dichotomously classify images as Aβ− or Aβ+, that is, the scan classification on which at least 3 of 5 interpreters agreed.

3D-SSP Implementation

The Montreal Neurologic Institute (MNI) standard space (*16,17*) together with an MR T1-weighted template from the International Consortium for Brain Mapping (ICBM) (*18*) were used as reference space. A binary brain mask was created based on the ICBM T1 template image. Triangulated surface models in MNI space corresponding to the whole brain and the left and right hemisphere were extracted from the binary brain mask using a marching cubes (*19*) algorithm. To receive more visually appealing surfaces than the original somewhat blocky surfaces generated by the marching cubes algorithm, the surfaces were smoothed using the Visualization Toolkit (*20*) implementation of a surface smoothing algorithm that prevents the surfaces from shrinking (*21*). Finally, for each surface point of the surface models the inverse surface normal was calculated.

The maximum projection depth for each surface point of the surface models was calculated individually. The rational for this was that the thickness of the cortex varies across the brain and that it is important to sample as much as possible of the cortex without entering the white matter that shows nonamyloid specific binding of ^{18}F-flutemetamol for both Aβ− and Aβ+ images. The variable maximum projection depth can be computed in different ways; in the method described here a ^{18}F-flutemetamol–negative template (*22*), intensity normalized to a region defined in the cerebellar cortex, was used.

A threshold for determining the border between gray and white matter was chosen by visual inspection in such way that it corresponded to the boundary of gray and white matter using the MNI space probabilistic gray and white matter masks provided with SPM8 (Wellcome Department of Cognitive Neurology, University College London) for guidance together with the ^{18}F-flutemetamol–negative template. A threshold value of 1.2 times the cerebellar cortex mean value was found to successfully discriminate white matter from gray matter in the ^{18}F-flutemetamol–negative template.

Before the individual depths were calculated, both a maximum depth, d_{max}, and a minimum depth, d_{min}, was chosen. The use of a minimum depth allows for compensation for atrophy or possible errors in the spatial normalization of the cortex. A large number of spatially normalized ^{18}F-flutemetamol and MR images were visually inspected, and it was concluded that the d_{max} set to 12 mm and d_{min} set to 2 mm were suitable.

The individual SSP maximum depth for each surface point was determined using the following criteria. Starting at the surface, the ^{18}F-flutemetamol–negative template was sampled with a fixed-step

length of 0.1 mm along the inverse surface normal until a value larger than the threshold was sampled or d_{max} was reached using the following criteria:

- If a value larger than the threshold is found, use the depth where this value is found as the SSP maximum depth for the current surface point.
- If no value larger than the threshold is found, use d_{max} as the SSP maximum depth for the current surface point.
- If a value larger than the threshold is found and its depth is less than the minimum depth, set the SSP maximum depth for this surface point to the minimum depth d_{min}.

In Figure 2 the calculated variable depth for SSP as defined above is illustrated. The red outer contour displays the whole-brain surface in which all surface points are defined, and the blue inner contour illustrates calculated SSP maximum depth for surface projections. The contours are displayed on the ^{18}F-flutemetamol–negative template used for calculating the variable depth.

All images from cohort 1 and 2 were spatially normalized to the MNI standard space with a specialized image registration method using an adaptive template for handling different uptake patterns in Aβ− and Aβ+ ^{18}F-flutemetamol images (*22*).

SUV ratio (SUVR) images (*23*) in standard space were created using all spatially normalized images from cohort 1 and 2. An SUVR image is obtained by dividing each voxel in the scan with the mean value of a reference region. In this study, the following 2 reference regions were used: the pons and cerebellar cortex.

A normal database was created using the SUVR images from cohort 1. For each image, the maximum SUVR, SSP_{max}, for each surface point of the surface models was calculated by sampling the image at a fixed-step length of 0.1 mm along the inverse surface normal, starting at the surface point going into the precalculated maximum depth associated to the point. With the SSP_{max} for each surface point for all healthy volunteers in cohort 1, the mean SSP_{max}, μ_{ref}, and SD for the SSP_{max}, σ_{ref}, for each surface point were calculated. These were then stored as the normal database for 3D-SSP.

With a normal database, a patient image can be compared with the normal database in the following way: for each surface point, the maximum SUVR intensity, SSP_{max}, can be calculated for the patient image in the same way as for the images contributing to the normal database. The SSP_{max} for each surface point can then be compared with the normal database as proposed by Minoshima et al. (*11*), that is, a z score can be calculated for each surface point according to Equation 1.

$$z = \frac{SSP_{max} - \mu_{ref}}{\sigma_{ref}}. \qquad \text{Eq. 1}$$

The z score represents the number of SDs a single patient is from the group mean.

Mapping the SSP_{max} directly onto its associated surface point of the 3D surfaces gives the 3D-SSP SUVR views of the image, whereas mapping the calculated z scores gives the 3D-SSP z score views of the image.

Visualization

A 3D rendering algorithm was implemented to visualize the 3D-SSP SUVR and z scores. The implementation allows fused display of the ^{18}F-flutemetamol image and the patient's MR image if available or the ICBM T1 template if the patient's MR image is not available. When displaying fused images, it is possible to blend the PET and the MR ranging from 100% PET to 100% MR. It is also possible to threshold the PET. SUVR and z score values below the threshold will be completely transparent, allowing the fused MR to show (Fig. 3).

If the patient's MR image is available, it can be transformed to the standard space along with the patient's ^{18}F-flutemetamol image. With the patient's MR image in standard space, its intensities can be projected onto the same 3D surfaces as for the ^{18}F-flutemetamol image. Because the 3D surface models are created in such a way that they are on the surface of the brain (except the medial part of the hemispheres),

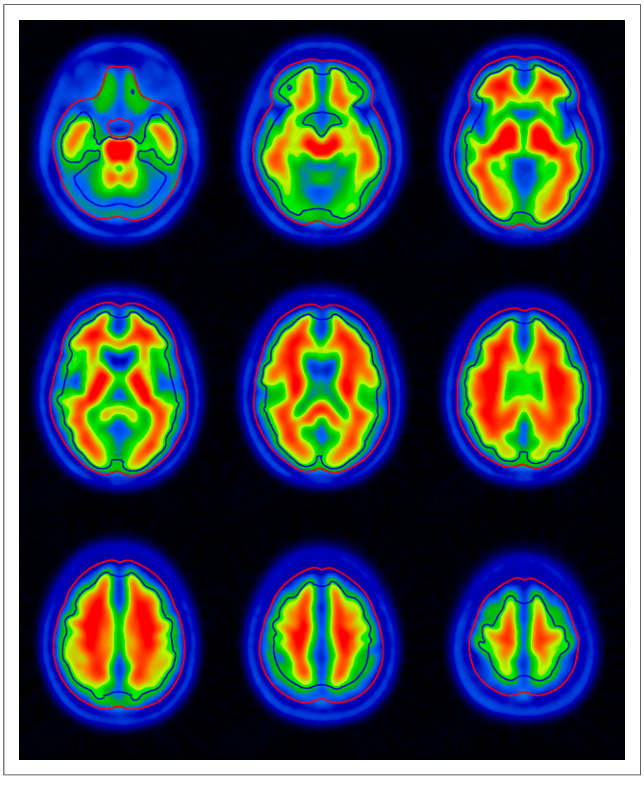

FIGURE 2. Variable-depth contour (blue) and brain surface contour (red) overlaid on ^{18}F-flutemetamol–negative template.

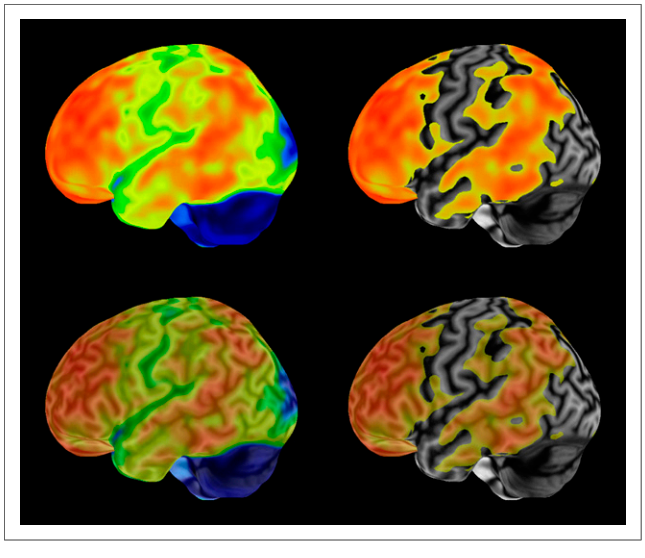

FIGURE 3. 3D-SSP maximum-intensity results of Aβ+ ^{18}F-flutemetamol image. (Upper left) PET values only. (Upper right) PET values with threshold set so that MR information is visible in areas in which PET values are below threshold. (Lower left) PET values with opacity set to 50%, revealing patient-specific MR information. (Lower right) PET values with opacity and threshold set.

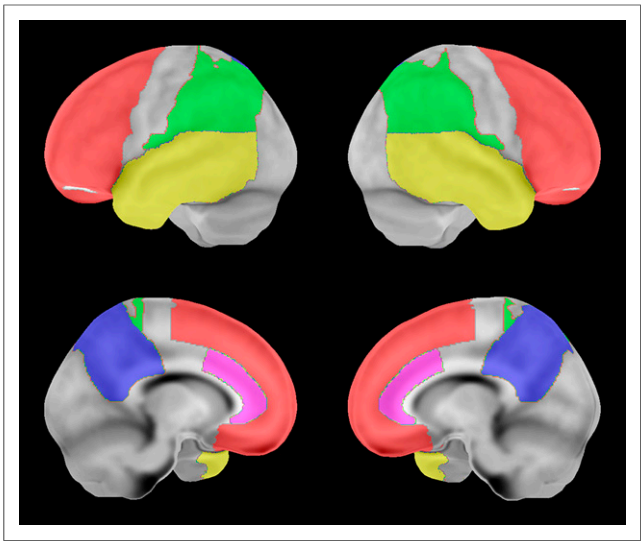

FIGURE 4. Surface regions used for cortical surface region: prefrontal, parietal, posterior cingulate, precuneus, temporal lateral, and anterior cingulate.

not much anatomic information of the brain is shown if the MR intensity values are taken from voxels corresponding to the points on the 3D surfaces. By visual inspection of a large set of MR images, it was concluded that a depth of 6 mm was suitable as a predetermined depth for the MR intensity projections, because it gave detailed anatomic information of the MR images as well as being deep enough to compensate for the possible registration errors and atrophy.

Experiments

A cortical surface region was created, based on several cortical regions from a volume-of-interest atlas derived from the automated anatomic labeling atlas (*24*). The following volumes of interest, known for having elevated uptake in amyloid-positive cases (*25,26*), were selected for the creation of the cortical surface region: prefrontal, parietal, posterior cingulate, precuneus, temporal lateral, and anterior cingulate. The surface region was created as follows: for each surface point, on the left and right hemispheres, the volume-of-interest atlas was sampled along the inverse surface normal into a predefined maximum depth of 10 mm. If any of the volumes of interest listed above was sampled, the surface point was labeled as part of a corresponding surface region (Fig. 4). Finally, a logic or operation was applied to all the surface regions to create the final cortical surface region.

For all surface points of the cortical surface region, retention ratios based on SSP_{max} were calculated for all SUVR images. With the retention ratios for all the surface regions for all images, z scores for cohort 2 could be calculated using the normal database created from cohort 1.

To evaluate the variable depth, an image was classified as Aβ− if the calculated z score for the cortical surface region had a value strictly lower than a predefined z score threshold. In the same way, an image was classified as Aβ+ if the calculated z score had a value equal to or higher than the predefined z score threshold.

A z score threshold, which was optimal for discriminating between Aβ− and Aβ+ images, was determined on the basis of the sensitivity and specificity in cohort 2 using the major interpreter agreement from the BIE as standard of truth. A receiver-operating-characteristic (ROC) analysis was performed, and the area under the curve (AUC) was calculated and used as a measure of the ability of the method to dichotomously classify the scans into Aβ− and Aβ+.

Statistical Analysis

Statistical analysis was performed using R (*27*), and ROC analysis was performed using the pROC plug-in (*28*).

RESULTS

One image in cohort 2 failed to register into template space because of prefrontal atrophy and was therefore excluded from the rest of the study, leaving a total of 171 images in cohort 2.

ROC analysis showed that both the pons and the cerebellar cortex separated standard of truth Aβ− and standard of truth Aβ+ images with an AUC of 1.00 (AUC_{pons} = 0.9997 and $AUC_{cerebellar\ cortex}$ = 0.9989). The optimal z score threshold using the pons as the reference region was calculated to 1.97, resulting in an overall visual read agreement in 170 of 171 images (99.42%) (Fig. 5). When the cerebellar cortex was used as the reference region, the optimal z score threshold was calculated to 2.41, resulting in an overall visual read agreement in 168 of 171 images (98.25%). The results of the ROC analysis are summarized in Table 1.

3D-SSP for Visual Assessment

Figure 6 shows 3 cases ranging from a typical Aβ− to a typical Aβ+. z scores are calculated using cerebellar cortex as reference region. z scores are presented using a rainbow color scale and

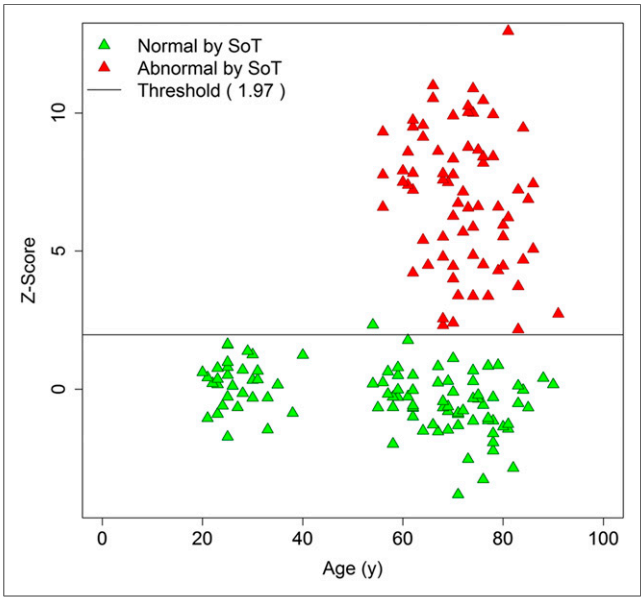

FIGURE 5. Cortical surface region z score for 171 subjects from cohort 2 plotted against age (pons as reference region). Calculated z score threshold of 1.97 gave concordance between quantitative and visual read in 170 of 171 images (99.42%). SoT = standard of truth, established by consensus from 5 experienced interpreters blinded to clinical data.

TABLE 1
Results of ROC Analyses

Reference region	z score threshold	Sensitivity	Specificity	AUC
Pons	1.97	1.00	0.99	1.0
Cerebellar cortex	2.41	0.99	0.98	1.0

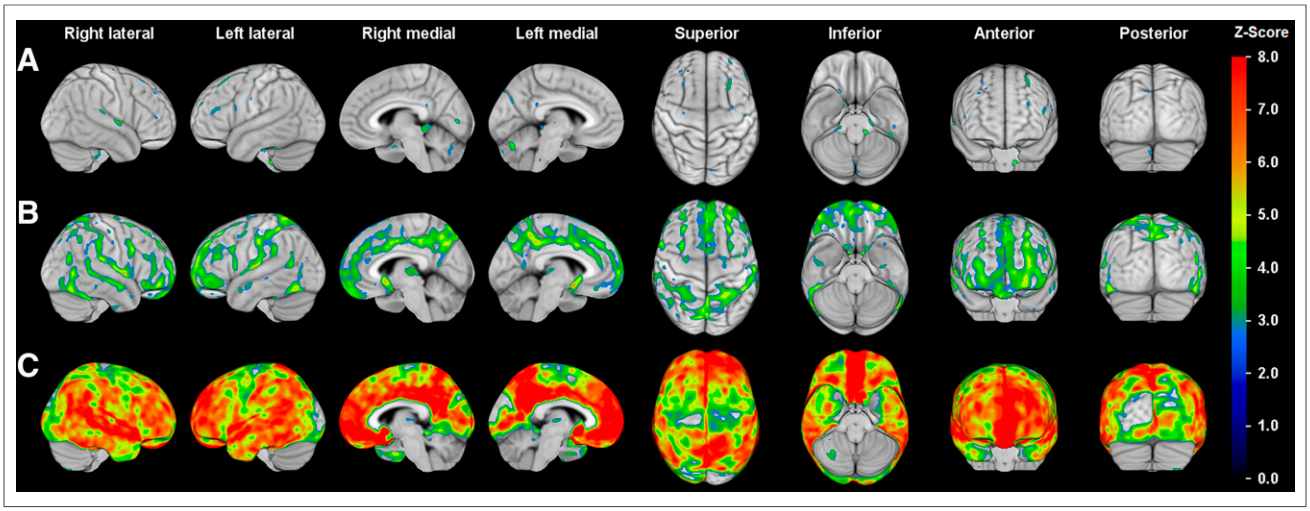

FIGURE 6. 3D-SSP z score images of 3 patients overlaid on ICBM T1 template (cerebellum as reference region). Threshold of $z = 2.0$ is applied, allowing MR to show where PET values are lower than $z = 2.0$. (A) Typical Aβ− case. (B) Image shows some typical AD patterns. (C) Typical Aβ+ case.

overlaid on the ICBM MR T1 template. A threshold of $z = 2.0$ is applied to all z score values, whereas z score values below the value 2.0 are completely transparent, thus revealing the MR template.

DISCUSSION

We implemented a variable-depth 3D-SSP method that is suitable for use with amyloid imaging data. We used a ^{18}F-flutemetamol–negative template to define the individual maximum depth for each 3D-SSP ray. We defined a cortical surface region and by averaging 3D-SSP points intersecting this surface region, we computed cortical SUVRs. We used a healthy cohort to define the reference range, and then we used a test cohort to evaluate the method by computing cortical z scores. We performed an ROC analysis and computed the AUC for the reference regions pons and cerebellar cortex, both yielding an AUC of 1.0. Our results showed that the method proposed in this study minimizes the sampling of white matter uptake, resulting in automated quantification and visualization with an accuracy of identifying pathologic uptake similar to that of BIE by trained observers. The combination of reliable quantification and didactic reporting presented here might be of relevance for more widespread adoption of amyloid imaging in clinical routine.

3D-SSP analysis still puts high demands on the spatial normalization to compensate for the different patterns in Aβ− and Aβ+ images. In this study, the use of the adaptive template spatial normalization strategy was considered essential to optimize the use of variable-depth 3D-SSP. This approach does not require MR or ^{18}F-FDG (*29*) from the same patient for registration to the template.

The presented method determines the individual maximum depth for each surface point using a threshold on a ^{18}F-flutemetamol–negative template. It may also be possible to define such individual maximum depth based on information from an average of several segmented MR images. However, because of partial-volume effects in PET images the use of MR-based methods to estimate the cortical thickness should be used with care. An age-correction factor for the individual maximum depth could also be relevant, because the thickness of the cortex decreases during normal aging, allowing the maximum depth applied in individual subject analysis to decrease with age.

The calculated z score threshold for defining a presence of amyloid was substantially higher when the cerebellar cortex was used as a reference, compared with the pons. This finding suggests a larger normal variation in the cerebellar cortical region of interest, and the results of this study would therefore point to the pons as the favored reference region. However, both structures were previously used as reference regions in studies of quantitative accuracy (*26,30,31*) with good results, suggesting that the graphical definition of the region has an impact. This study found only an insignificantly higher accuracy referencing pons, and even larger and prospective studies would be needed to determine a preference for either structure. In clinical practice, however, access to an automated implementation of both approaches might be useful for confirmation in certain cases.

In clinical practice today, the detection of cerebral amyloidosis based on PET is dichotomous, and a quantitative approach with a set cutoff might help the reviewing physician to reduce ambiguous reporting in borderline cases. This study confirmed that both the pons and the cerebellar cortex are useful as reference regions for SUVR calculations, and the high accuracy of the method, compared with trained interpreters in a validated material, is encouraging. In addition to the visual appeal of whole-brain presentation, 3D-SSP applied to amyloid PET might therefore become a useful adjunct tool for more inexperienced interpreters, which, however, requires further validating studies. Even though 3D-SSP images were carefully inspected visually during the development of the described method and quantitative results showed excellent agreement with BIE, which in turn was validated against autopsy-derived levels of amyloid, it is suggested that further studies should be performed potentially based only on the 3D-SSP or in a combination of a traditional BIE to prospectively evaluate the diagnostic value of the method. The proposed method is potentially applicable to other amyloid tracers but should be evaluated with tracer-specific templates.

CONCLUSION

The described variable-depth 3D-SSP method allows for computation of ^{18}F-flutemetamol 3D-SSP maps in which contribution from white matter signal is minimized while retaining

sensitivity in detecting gray matter signal. Further studies are needed to evaluate the impact of the method for amyloid imaging in clinical routine.

DISCLOSURE

The costs of publication of this article were defrayed in part by the payment of page charges. Therefore, and solely to indicate this fact, this article is hereby marked "advertisement" in accordance with 18 USC section 1734. Johan Lilja and Lennart Thurfjell were, during the time of the study, employed by GE Healthcare, owner of the ^{18}F-flutemetamol label. No other potential conflict of interest relevant to this article was reported.

REFERENCES

1. Alzheimer's Association. 2014 Alzheimers disease facts and figures. *Alzheimers Dement.* 2014;10:e47–e92.
2. Anand R, Gill KD, Mahdi AA. Therapeutics of Alzheimer's disease: past, present and future. *Neuropharmacology.* 2014;76:27–50.
3. Klunk WE, Engler H, Nordberg A, et al. Imaging brain amyloid in Alzheimer's disease with Pittsburgh compound-B. *Ann Neurol.* 2004;55:306–319.
4. Wong DF, Rosenberg PB, Zhou Y, et al. In vivo imaging of amyloid deposition in Alzheimer disease using the radioligand ^{18}F-AV-45 (florbetapir [corrected] F 18). *J Nucl Med.* 2010;51:913–920.
5. Clark CM, Schneider JA, Bedell BJ, et al. Use of florbetapir-PET for imaging beta-amyloid pathology. *JAMA.* 2011;305:275–283.
6. Barthel H, Gertz H-J, Dresel S, et al. Cerebral amyloid-β PET with florbetaben (^{18}F) in patients with Alzheimer's disease and healthy controls: a multicentre phase 2 diagnostic study. *Lancet Neurol.* 2011;10:424–435.
7. Villemagne VL, Ong K, Mulligan RS, et al. Amyloid imaging with ^{18}F-florbetaben in Alzheimer disease and other dementias. *J Nucl Med.* 2011;52:1210–1217.
8. Nelissen N, Van Laere K, Thurfjell L, et al. Phase 1 study of the Pittsburgh compound B derivative ^{18}F-flutemetamol in healthy volunteers and patients with probable Alzheimer disease. *J Nucl Med.* 2009;50:1251–1259.
9. Vandenberghe R, Van Laere K, Ivanoiu A, et al. ^{18}F-flutemetamol amyloid imaging in Alzheimer disease and mild cognitive impairment a phase 2 trial. *Ann Neurol.* 2010;68:319–329.
10. Rowe CC, Pejoska S, Mulligan RS, et al. Head-to-head comparison of ^{11}C-PiB and ^{18}F-AZD4694 (NAV4694) for β-amyloid imaging in aging and dementia. *J Nucl Med.* 2013;54:880–886.
11. Minoshima S, Frey KA, Koeppe RA, Foster NL, Kuhl DE. A diagnostic approach in Alzheimer's disease using three-dimensional stereotactic surface projections of fluorine-18-FDG PET. *J Nucl Med.* 1995;36:1238–1248.
12. Lehman VT, Carter RE, Claassen DO, et al. Visual assessment versus quantitative three-dimensional stereotactic surface projection fluorodeoxyglucose positron emission tomography for detection of mild cognitive impairment and Alzheimer disease. *Clin Nucl Med.* 2012;37:721–726.
13. Adamczuk K, De Weer A-S, Nelissen N, et al. Polymorphism of brain derived neurotrophic factor influences β amyloid load in cognitively intact apolipoprotein E ε4 carriers. *Neuroimage Clin.* 2013;2:512–520.
14. Bridging Study of C11 PiB and F18 Flutemetamol Brain PET. ClinicalTrials.gov website. http://clinicaltrials.gov/show/NCT01607476. Accessed March 17, 2016.
15. European Medicines Agency. Vizamyl. European Medicines Agency website. http://www.ema.europa.eu/ema/index.jsp?curl=pages/medicines/human/medicines/002557/human_med_001794.jsp&mid=WC0b01ac058001d124. Updated October 11, 2015. Accessed March 17, 2016.
16. Evans AC, Collins DL, Mills SR, Brown ED, Kelly RL, Peters TM. 3D statistical neuroanatomical models from 305 MRI volumes. *IEEE Nucl Sci Symp Med Imaging Conf Rec.* 1993:1813–1817.
17. Fonov V, Evans AC, Botteron K, Almli CR, McKinstry RC, Collins DL. Unbiased average age-appropriate atlases for pediatric studies. *Neuroimage.* 2011;54:313–327.
18. ICBM-152 template. ICBM website. http://packages.bic.mni.mcgill.ca/tgz/mni-models_icbm152-lin-1.0.tar.gz. Accessed April 26, 2016.
19. Lorensen WE, Cline HE. Marching cubes: a high resolution 3D surface construction algorithm. *Computer Graphics.* 1987;21:163–169.
20. Vizualization Toolkit. VTK website. http://www.vtk.org. Accessed March 17, 2016.
21. Taubin G. Curve and surface smoothing without shrinkage. In: *Proceedings of IEEE International Conference on Computer Vision*. 1995:852–857.
22. Lundqvist R, Lilja J, Thomas BA, et al. Implementation and validation of an adaptive template registration method for ^{18}F-flutemetamol imaging data. *J Nucl Med.* 2013;54:1472–1478.
23. Lopresti BJ, Klunk WE, Mathis CA, et al. Simplified quantification of Pittsburgh compound B amyloid imaging PET studies: a comparative analysis. *J Nucl Med.* 2005;46:1959–1972.
24. Tzourio-Mazoyer N, Landeau B, Papathanassiou D, et al. Automated anatomical labeling of activations in SPM using a macroscopic anatomical parcellation of the MNI MRI single-subject brain. *Neuroimage.* 2002;15:273–289.
25. Braak H, Braak E. Neuropathological stageing of Alzheimer-related changes. *Acta Neuropathol (Berl).* 1991;82:239–259.
26. Thurfjell L, Lilja J, Lundqvist R, et al. Automated quantification of ^{18}F-flutemetamol PET activity for categorizing scans as negative or positive for brain amyloid: concordance with visual image reads. *J Nucl Med.* 2014;55:1623–1628.
27. The R Project for Statistical Computing. R Foundation website. http://www.r-project.org/. Accessed March 17, 2016.
28. Robin X, Turck N, Hainard A, et al. pROC: an open-source package for R and S+ to analyze and compare ROC curves. *BMC Bioinformatics.* 2011;12:77.
29. Kaneta T, Okamura N, Minoshima S, et al. A modified method of 3D-SSP analysis for amyloid PET imaging using [^{11}C]BF-227. *Ann Nucl Med.* 2011;25:732–739.
30. Hatashita S, Yamasaki H, Suzuki Y, Tanaka K, Wakebe D, Hayakawa H. ^{18}F flutemetamol amyloid-beta PET imaging compared with [^{11}C]PIB across the spectrum of Alzheimer's disease. *Eur J Nucl Med Mol Imaging.* 2014;41:290–300.
31. Leinonen V, Rinne JO, Wong DF, et al. Diagnostic effectiveness of quantitative [^{18}F]flutemetamol PET imaging for detection of fibrillar amyloid β using cortical biopsy histopathology as the standard of truth in subjects with idiopathic normal pressure hydrocephalus. *Acta Neuropathol Commun.* 2014;2:46.